ACS Catalysis

pubs.acs.org/acscatalysis
Research Article

Benchtop-Stable Carbyl Iminopyridyl Ni^{II} Complexes for Olefin Polymerization

Hasaan S. Rauf, Yu-Sheng Liu, Muhammad Arslan, Surya Pratap S. Solanki, Eric Deydier, Rinaldo Poli,* Lars C. Grabow,* and Eva Harth*

Cite This: ACS Catal. 2024, 14, 13136−13147
Read Online

ACCESS | Metrics & More | Article Recommendations | Supporting Information

ABSTRACT: Design of catalysts for Ni-catalyzed olefin polymerization predominantly focuses on ligand design rather than the activation process when attempting to achieve a broader scope of polyolefin micro- and macrostructures. Air-stable alkyl-or aryl-functionalized Ni^{II} precatalysts were designed which eliminate the need of in situ alkylating processes and are activated solely by halide abstraction to generate the cationic complex for olefin polymerization. These complexes represent an emerging class of olefin polymerization catalysts, enabling the study of various cocatalysts forming either inner- or outer-sphere ion pairs. It is demonstrated that an organoboron cocatalyst activation produces a well-defined ion pair, which in contrast to ill-defined organoaluminum cocatalysts, can directly activate the complex by halide abstraction to yield comparatively higher molecular weight homo/copolymers. Under high ethylene pressure, broader branching densities and the gradual incorporation of short-chain branches were achieved, circumventing the need for elaborate ligand design and copolymerization with α-olefins. The underlying chain-walking mechanism and ion pair interactions were further elucidated by DFT calculations. A phenyl group on the bridging carbon functioned as a rotational barrier, producing higher molecular weight polymers compared to methyl-substituted analogs. Here, we provide a perspective to manipulate the iminopyridyl Ni^{II} system, leveraging ion pair interactions and ligand design to govern polyolefin molecular weights and microstructures.

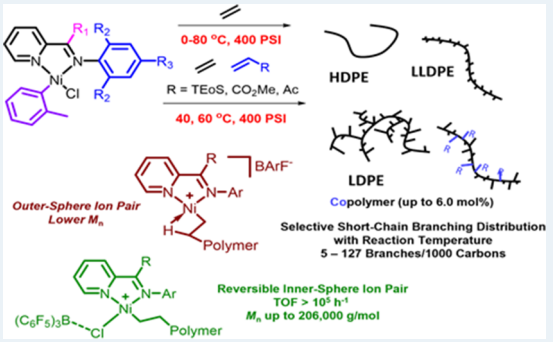

KEYWORDS: *catalysis, ion pairs, olefin polymerization, iminopyridyl nickel complexes, organoboron cocatalyst*

INTRODUCTION

The success of polymeric materials is rooted in their versatility, high performance, and affordable production.[1−3] Among these materials, polyolefins continue to make up about half of the polymer production due to their exceptional chemical resistance and tunable material properties.[4] In general, the physical properties of polyolefins are directly related to their molecular weight (MW) and microstructure, which is highly dependent on the involved catalytic system. Over the years, there has been a surge in the development of ligands aimed at the control of the polymer microstructure to influence material properties. However, effective microstructure control has required the use of increasingly complex ligands.[5]

Olefin polymerization systems rely not only on the transition metal complex but also on the cocatalyst used for activation.[6−9] The ionic interaction between the metal complex and the counterion significantly impacts the catalytic activity and polymer architecture in early transition metal-catalyzed olefin polymerizations.[10−14] For olefin polymerization reactions, this cation−anion interaction can exist as either inner- or outer-sphere ion pairs. Using well-defined alkyl-abstracting organoboron cocatalysts to activate zirconocene complexes, such as tris(pentafluorophenyl)borane ($B(C_6F_5)_3$) and triphenylcarbenium tetraphenylborate (TBCF), showed dramatic differences in catalytic activity and stereoselectivity.[15] The difference in the catalytic activity using these organoboron cocatalysts was attributed to the notion that smaller counterions favored inner-sphere ion pairs, which could compete with monomer coordination and reduce catalytic activity, and bulkier counterions preferred noncoordinating outer-sphere ion pairs, increasing catalytic activity (Figure 1A).[10,16]

The development of the Brookhart-type catalysts launched the field of late-transition metal-catalyzed olefin polymerization (Figure 1B).[17] While these α-diimine Pd^{II} and Ni^{II} complexes are highly tolerant of polar monomers and provide control over polymer microstructure through their unique "chain-walking" mechanism, investigations into the effect of the influence of the counterion for these catalytic systems are limited.[18] Diimine Pd^{II}/Ni^{II} complexes can be designed with halide and carbyl

Received: May 20, 2024
Revised: August 12, 2024
Accepted: August 13, 2024
Published: August 16, 2024

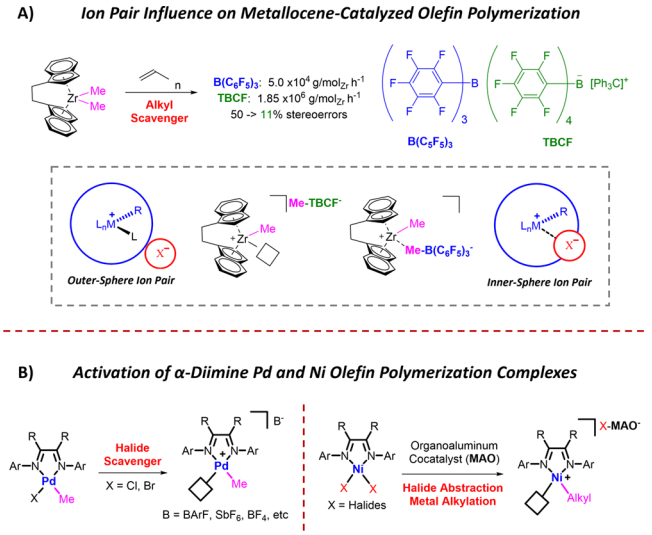

Figure 1. Ion pairs for olefin polymerization. (A) Activation of early transition metal complexes using alkyl abstracting inner- and outer-sphere counterions in comparison to (B) activation of α-diimine Pd complexes with halide abstracting activators and in-situ activation of α-diimine Ni complexes by halide abstracting/alkylating organoaluminum cocatalyst methylaluminoxane (MAO).

ligands for activation by both organoaluminum and organoboron cocatalysts.[11]

Although alkylated diimine Ni complexes exist, they can suffer from poor stability.[19,20,13] For example, in 1980, Dieck reported that diimine Ni dimethyl complexes are stable up to 0 °C.[21,22] Switching to the sterically bulkier alkyl group, R = CH_2SiMe_3 exhibits higher thermal stability; however, comprehensive activation and polymerization studies have not been reported.[23] Highly stable alkylated Ni complexes for polymerization remain elusive.

Diimine Ni^{II} analogs intended for olefin polymerization reactions were predominantly designed containing dihalide ligands limiting the activation to bifunctional organoaluminum cocatalysts such as methylaluminoxane (MAO), which functions through halide abstraction and metal alkylation for coordination insertion polymerization. Unfortunately, there are few catalytic systems that allow for the investigation of counterion effects in [*N*,*N*]-chelated Ni^{II} complexes. For instance, only two cationic carbyl diimine Ni^{II} complexes are reported for olefin polymerization due to lability of the Ni−C bond, rendering them thermally unstable (Figure 2A).[10,17] Similarly, η^3-coordinated cationic diimine Ni complexes isolated with a PF_6^- anion, are temperature sensitive and also require organoaluminum cocatalysts for olefin polymerization (Figure 2B).[24] Alkylsilane substituted diimine Ni complexes which could copolymerize ethylene and vinyltrialkoxysilanes require an activation with a combination of $B(C_6F_5)_3$ and $Li(B(C_6F_5)_4)$ and are also air-sensitive (Figure 2C).[25] While thermally sensitive dimethyl diimine Ni complexes have been reported, they are limited to activation with organoboron cocatalysts which abstract an alkyl group to afford the cationic active species (Figure 2D).[21]

Meanwhile, the activation through MAO limits the in-depth study on the influence of cocatalysts and reaction conditions to tailor polymer microstructures due to limited understanding of the anionic macrostructure of MAO.[26] The ability to investigate inner- and outer-sphere ion pairs to govern polymeric properties is contingent upon a carbyl Ni precatalyst.[11] Therefore, it is crucial to develop a robust carbyl Ni^{II} precatalyst activatable by a variety of cocatalysts to evaluate the impact of counterions on [*N*,*N*]-chelated Ni^{II} complexes, because the catalytic activity and the type of polymeric material produced can be influenced by the activation method and the choice of cocatalyst.[27−30] The

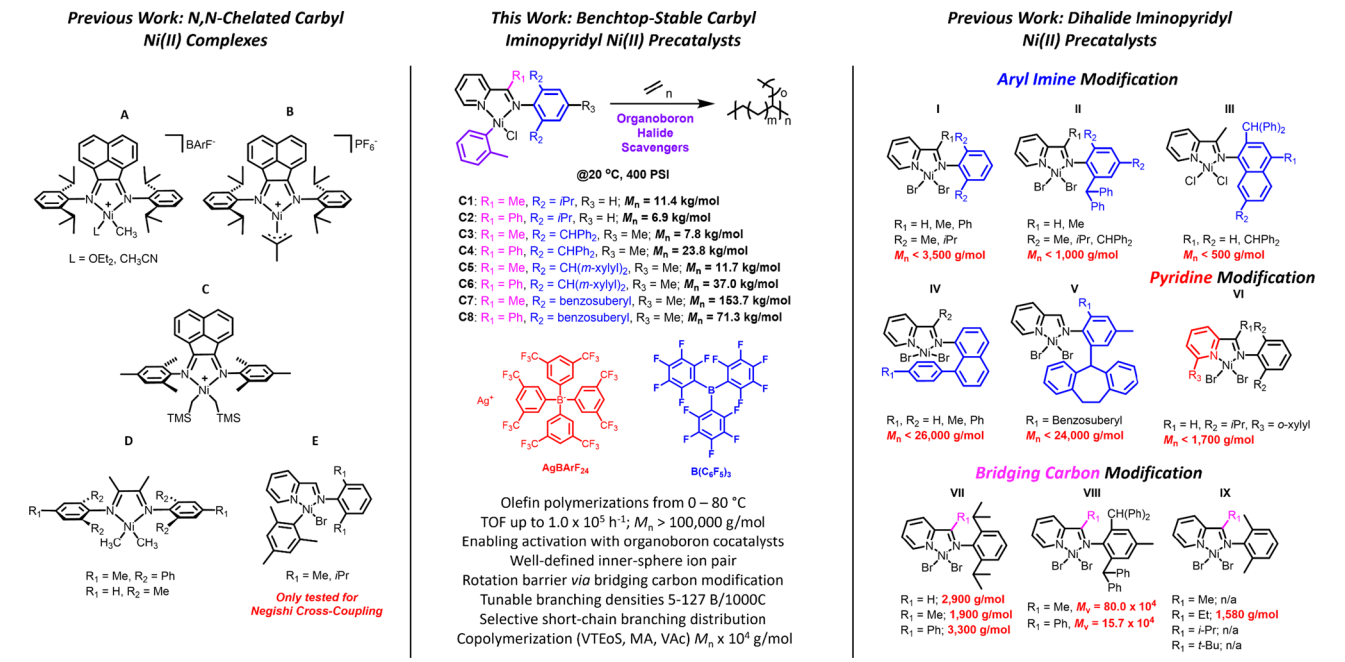

Figure 2. Selected examples of [*N*,*N*]-chelated nickel olefin polymerization complexes. Carbyl [N,N]-chelated Ni complexes **A**−**E** and dihalide iminopyridyl Ni complexes with aryl imine (I−V), pyridine (VI), and bridging carbon (VII−IX) modifications. In this work, benchtop-stable carbyl iminopyridyl Ni^{II} complexes are reported.

https://doi.org/10.1021/acscatal.4c02708
ACS Catal. 2024, 14, 13136−13147

shift from intricate ligand design to utilization of ion pairs could offer control over polymer microstructure and MW.

Specifically, we seek to create an aryl-functionalized Ni precatalyst, activated solely by a halide abstraction, eliminating the need for an alkylation process to generate the cationic complex for olefin polymerization. These complexes would serve as an ideal system for a variety of activators, expanding beyond the limitation of organoaluminum cocatalysts. Thus, we selected iminopyridine ligands, with the [*N*,*N*]-ligand backbone serving as a diimine analog and the pyridine moiety acting as a stronger σ-donor to stabilize the labile Ni−C bond.[31] Notably, benchtop-stable iminopyridyl mesityl Ni^{II} complexes have been prepared (Figure 2E) for use in Negishi cross-coupling reactions.[32] Iminopyridine ligands have been extensively used in olefin polymerization, with the Ni complexes exhibited similar catalytic activity compared to their α-diimine analogues.

However, traditional ligand design focusing on increasing steric bulk on the aryl imine produced lower MW polymers, seemingly contradicting the established trend reported for late-transition metal complexes where increasing axial steric bulk on the metal center favored chain-propagation and yielded higher MW polymers (Figure 2I−III).[33−36] We hypothesize that the steric bulk of the single aryl imine moiety cannot sufficiently contribute to the effective blockage of the metal center to limit chain-transfer. These complexes could produce moderate MW polyethylene (PEs) (M_n < 26,000 g mol^{-1}) at ambient conditions with the development of the "half-sandwich" iminopyridine ligands (Figure 2IV), where the "aryl cap" of the 8-arylnaphthyl imine aggressively shielded a single axial site.[37] Guo and Dai later introduced a rotation-restricted strategy using rigid benzosuberyl substituents (Figure 2V), enhancing axial shielding and yielding moderate MW PEs (M_n < 24,000 g mol^{-1}) and high MW PEs when combined with the "half-sandwich" scaffold.[38−41] Alternatively, substituents at the 6-position of the pyridine (Figure 2VI) increased the mol % incorporation of polar monomers, but occupy the same coordination plane as ethylene and the growing polymer chain, promoting chain-transfer and the production of low MW PEs and oligomers. (M_n < 1700 g mol^{-1}).[42,43]

Therefore, we sought to explore the impact of steric bulk on the substituent on the imino-carbon, commonly referred as bridging carbon, by introducing a phenyl group as a "rotational barrier", which would restrict the aryl imine substituents in their mobility and increase axial bulk to limit chain-transfer. Surprisingly, few iminopyridyl Ni complexes have been designed with substituents other than a hydrogen or methyl group on the carbon.[44] Laine et al. varied the bulk with hydrogen, methyl, and phenyl groups, but the MW was inconsistent with the steric bulk (Figure 2VII).[45] Zohuri and co-workers found that replacing the methyl bridging substituent with a phenyl group led to a significant decrease in M_v, suggesting bulkier bridging carbon substituents negatively affect polymerization (Figure 2VIII).[46] Zubris and co-workers alternatively explored alkyl groups on the bridging carbon but only produced low MW polymers (M_n < 1600 g mol^{-1}) with an ethyl substituent (Figure 2IX).[47]

In this contribution, we disclose the synthesis of an emerging class of benchtop, air-stable iminopyridyl Ni^{II} complexes, **C1**−**C8**, which feature an *o*-tolyl ligand as the carbyl substituent as the aryl ligand has been found to produce benchtop-stable bipyridine Ni^{II} complexes.[31] We investigate the significance and effect of the ion pair for ethylene polymerization, and its role in tailoring branching characteristics and density of the produced PE with respect to the reaction conditions. The complexes are designed with a focus on a rotational barrier provided by either a methyl or phenyl group on the bridging carbon and the *ortho*-substituents on the aryl imine. Various cocatalysts such as modified-MAO, sodium tetrakis[3,5-bis(trifluoromethyl) phenyl]borate (NaBArF), silver tetrakis-[3,5-bis(trifluoromethyl) phenyl]borate (AgBArF), and organoboranes were evaluated for ethylene polymerization. Furthermore, we demonstrate the use of $B(C_6F_5)_3$ as the primary cocatalyst for carbyl Ni^{II} iminopyridyl complexes, producing active complexes and yielding high MW PE (M_n > 100 kg mol^{-1}) compared to known nonhalf sandwich and half-sandwich iminopydridyl complexes.

Density functional theory (DFT) studies support the establishment of a reversible inner-sphere anion coordination with $ClB(C_6F_5)_3^-$, which reduces the overall catalytic activity, but allows the production of higher MW polymers. Moreover, the activation of these complexes with $B(C_6F_5)_3$ allows for the study that the substituent on the bridging carbon greatly influences the polymer MWs through a rotational restriction of the *ortho*-substituents on the aryl imine moiety. The chain-walking behavior leads to controlled branching densities and short-chain branching distributions, ranging from methyl to butyl, depending on the reaction temperature (0−80 °C), producing polymers with diverse macrostructures. DFT studies also support a proposed mechanistic pathway to elucidate the underlying chain-walking mechanism. Complex **C7** is used to evaluate the efficacy of the carbyl iminopyridyl Ni complexes for copolymerization with polar monomers. In addition, a single catalyst can generate several types of PEs, such as high-density PE (HDPE), linear low-density PE (LLDPE), and low-density PE (LDPE) with controlled branching densities, circumventing the need for copolymerization with α-olefins. These carbyl Ni^{II} iminopyridyl complexes are competitive catalysts for olefin polymerization in which not only the MW but also the microstructure can be tuned by cocatalyst selection and ligand design, which is desired for a one-complex/one-monomer catalytic system.

RESULTS AND DISCUSSION

Design and Development of Carbyl Iminopyridyl Nickel Catalysts. A series of iminopyridine ligands (**L1**−**L8**) were synthesized using a one-step condensation reaction of the aniline with the targeted ketone and were isolated in high yields (Figure 3a).[34,45,46,48,49] Ligands **L1**, **L3**, **L5**, and **L7** feature a methyl group on the bridging carbon atom and a varied steric bulk on the aryl imine moiety, ranging from isopropyl to benzosuberyl groups, whereas ligands **L2**, **L4**, **L6**, and **L8** have a phenyl group on the bridging carbon. Notably, the *m*-xylyl substituents (**L5** and **L6**) and the benzosuberyl substituent (**L7** and **L8**) have only been investigated in iminopyridyl Pd complexes with a methyl group on the bridging carbon.[50] The complexations were achieved either by ligand exchange using $(PPh_3)_2Ni(o\text{-Tol})Cl$ or by oxidative addition with $Ni(COD)_2$ and 2-chlorotoluene (Figure 3b), forming iminopyridyl Ni^{II} catalysts **C1**−**C8** in good yields (66−92% for **C1**−**C7** and 10% for **C8**, Figure S2). We found that the more traditional route using $Ni(COD)_2$ imposed challenges and resulted in low yielding reactions. In contrast, the alternative route using ligand exchange between a commercially available nickel precursor ($(PPh_3)_2Ni(o\text{-Tol})Cl$)

https://doi.org/10.1021/acscatal.4c02708
ACS Catal. 2024, 14, 13136−13147

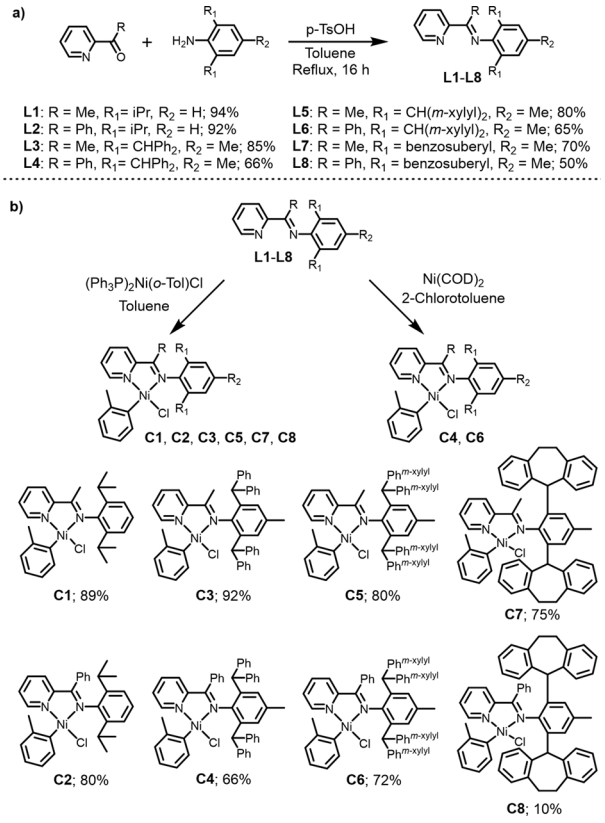

Figure 3. Synthesis of carbyl iminopyridyl Ni^{II} complexes. (a) Synthesis of iminopyridine ligands **L1**−**L8**. (b) Complexation of ligands to form Ni^{II} catalysts **C1**−**C8**.

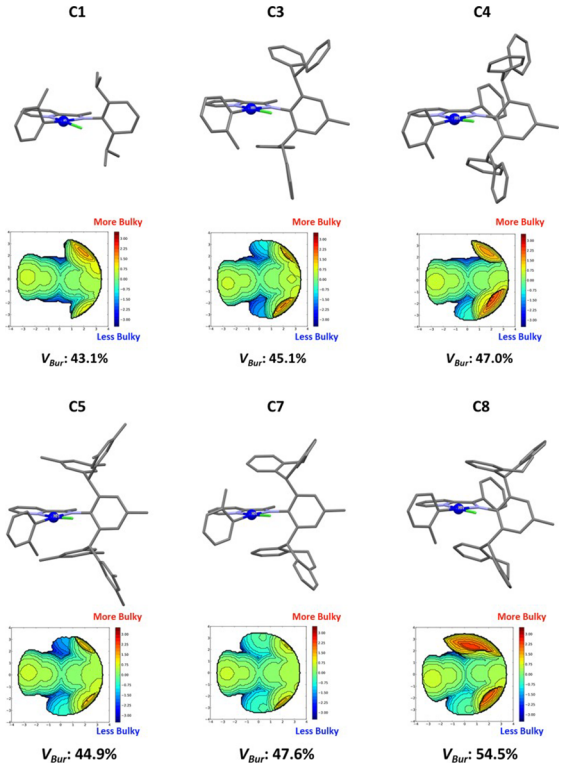

Figure 4. X-ray structures of carbyl iminopyridyl Ni^{II} complexes. Stick models, steric maps, and V_{Bur}% of **C1**, **C3**, **C4**, **C5**, **C7**, and **C8**.

and the iminopyridine was more practical for the majority of the complexes with the exception of **C4** and **C6** which achieved higher yields using the $Ni(COD)_2$ oxidative addition pathway.

The structures of **C1**, **C3**, **C4**, **C5**, **C7**, and **C8** were determined by single-crystal X-ray diffraction, revealing in all cases square planar geometries (Figure 4). In addition, the square planar configuration allowed for Ni^{II} complexes **C1**-**C7** to be fully characterized by ^1H NMR and ^{13}C NMR (Figures S3−S20). The topographic steric maps quantify the steric effect on the metal center imposed by the rotational barrier of the bridging carbon on the aryl imine substituents.[51] Catalysts **C1**, **C3**, **C5** and **C7** illustrate the steric influence provided by the aryl imine moiety on the blockage of the metal center. However, the inclusion of the phenyl group on the bridging carbon atom increases the buried volume percentage to 47.0% for **C4** and 54.5% for **C8** compared to their methyl analogues (45.1% for **C3** and 47.6% for **C7**). These data support our hypothesis that the substituent on the bridging carbon atom can introduce a rotational barrier, enhancing the shielding of the metal center. This is achieved by constraining the rotation of the *ortho*-aryl imine substituents, thereby imposing greater axial bulk and potentially retarding chain-transfer mechanisms.

Air- and Moisture Stability. During the synthesis of the complex series, we noticed a stability and robustness in atmospheric environments. Therefore, we thought to conduct a more detailed study to confirm their benchtop stability. Complexes **C1** and **C3** were selected as representative complexes for air- and moisture stability tests. Here, we subjected the complexes to open air and were analyzed by ^1H NMR spectroscopy for any signs of degradation. After 3 weeks of taking aliquots, we did not find any decomposition or degradation of complexes (Figures S150 and S151). A vigorous moisture sensitivity test was conducted by treating the complexes with excessive amounts of pure water. The ^1H NMR analysis of the dried crude samples showed a decomplexation of **C1** of only 13.4% and 18% for **C3** (Figures S152 and S153). These studies illustrate the high stability of the complexes and were therefore referred to as "benchtop" stable.

Cocatalyst Study. We selected **C1** as a model to study the counterion effect for ethylene polymerization by using various cocatalysts. Preliminary polymerizations with **C1** were conducted by in situ activation with modified-MAO (MMAO) and diethylaluminum chloride (Et_2AlCl) at 20 °C (Table 1, **entry 1, 2**). The MW of the polymers was analyzed using high-temperature gel permeation chromatography (HT-GPC) and was found to be 6.5 and 4.0 kg mol^{-1}, respectively. Although the organoaluminum cocatalysts produced a highly active species (TOF > 535,700 h^{-1}), the polymerization reaction resulted in a higher dispersity ($Đ$ = 2.47 and 2.11) for the isolated polymers. The in situ activation of C1 with NaBArF produced PE with higher MW (M_n = 8.5 kg mol^{-1}, Table 1, **entry 3**). However, the catalytic activity was poor (TOF = 12,900 h^{-1}). We suggest that the sodium cation is unable to efficiently abstract the halide from the metal center, leading to lower productivity. The poor activity was addressed with AgBArF, which produces AgCl with greater lattice energy than NaCl, implying a stronger halide abstraction.[52] Activating with AgBArF produced a 12 times more active catalyst (TOF = 162,900 h^{-1}), but reduced the polymer MW to 6.4 kg mol^{-1} (Table 1, entry 4). Other commonly used cocatalysts, such as $NaBF_4$ and $AgPF_6$, were investigated but were found to produce no polymer, illustrating the significant impact the ion

https://doi.org/10.1021/acscatal.4c02708
ACS Catal. 2024, 14, 13136−13147

Table 1. Ethylene Polymerization of C1 with Different Cocatalysts[a]

entry	cocatalyst	time (min)	yield (g)	productivity (kg mol$^{-1}_{Ni}$ h)	TOF (10^3)(h^{-1})	B/1000C[b]	M_n[c] (kg mol^{-1})	$Đ$[c]	T_m[d] (°C)
1[e]	MMAO (200 equiv)	5	3.0	18,000	642.9	27	6.5	2.47	109.3
2[e]	Et_2AlCl (200 equiv)	5	2.5	15,000	535.7	40	4.0	2.11	102.7
3	NaBArF (1.2 equiv)	10	0.3	360	12.9	26	8.5	1.98	108.3
4	AgBArF (1.2 equiv)	10	3.8	4560	162.9	32	6.4	2.00	105.2
5[f]	AgBArF (1.2 equiv)	5	3.2	7680	274.3	41	4.6	2.17	104.6
6	$B(C_6F_5)_3$ (10 equiv)	10	2.4	2880	102.9	25	11.4	1.93	108.6

[a]Conditions: 5 μmol of **C1**, 400 psi ethylene, 45 mL of toluene, 20 °C. [b]Determined by ^{1}H NMR in D_2-tetrachloroethane at 125 °C. [c]Determined by GPC in 1,2,4-trichlorobenzene at 160 °C using polystyrene calibration. [d]Determined by differential scanning calorimetry. [e]2 μmol of **C1**. [f]Included 10 equiv of $B(C_6F_5)_3$. TOF = Turnover Frequency, M_n = Number-Average Molecular Weight, $Đ$ = Dispersity, T_m = Melting Temperature.

pair has on olefin polymerization. To further enhance catalytic activity, ($B(C_6F_5)_3$) was used as an additive, with reports showing that the organoborane promotes ethylene polymerizations with diimine Ni^{II} catalysts.[53] Although the sequential addition of both $B(C_6F_5)_3$ and AgBArF significantly increased the activity of C1 (TOF = 274,300 h^{-1}), the MW of the resulting PE decreased to 4.6 kg mol^{-1} (Table 1, **entry 5**). While the dispersity remained consistent when only using AgBArF, it increased to 2.17 with the addition of $B(C_6F_5)_3$. This increase in dispersity suggested a simultaneous addition of AgBArF and $B(C_6F_5)_3$ could generate active species with differing ion pairs. Remarkably, activating **C1** with only $B(C_6F_5)_3$ produced PE with the highest MW for the tested cocatalysts (M_n = 11.4 kg mol^{-1}) and exhibited good catalytic activity and lowest dispersity (TOF = 102,900 h^{-1}, $Đ$ = 1.93, Table 1, **entry 6**). We hypothesized that the $B(C_6F_5)_3$ can abstract the halide and generate the $B(C_6F_5)_3$-Cl anion. For instance, Erker and Le Gendre[54] showed that BCF selectively abstracts a chloride from titanecene complexes generating a frustrated Lewis pair with a $B(C_6F_5)_3$-Cl anion which has an inner-sphere coordination. This report motivated us to investigate if a similar phenomenon occurs with our complexes. Therefore, a ^{19}F NMR was conducted and a shift in all three peaks of the fluorenes of $B(C_6F_5)_3$ was observed which implies the formation of $B(C_6F_5)_3$-Cl (Figure S149). Additionally, we believe that aryl ligand abstraction by $B(C_6F_5)_3$ is unlikely for two reasons: Ni(I) halides complexes are not known to initiate polymerization, and Ni(I) halides tend to dimerize, and such dimers are very stable and therefore catalytically inactive. For these reasons, we strongly believe that the $B(C_6F_5)_3$ activates the complex by halide abstraction.

In transition metal polymerization catalysis, it is known that inner- or outer-sphere ion pairing is attributed to different catalytic activity of the metal center. During polymerization, monomer insertion occurs at the open site of the active catalyst; however this coordination site can be occupied by the cocatalyst.[55] Weakly coordinating anions, such as $BArF^-$, should prefer outer-sphere ion pairs, facilitating monomer coordination and higher catalytic activity.[56] However, this leads to the more β-CH agostic species, which can lead to chain-transfer to monomer by β-H elimination and lower MWs, as observed experimentally with the activation of **C1** with AgBArF. Activation with $B(C_6F_5)_3$ produces $ClB(C_6F_5)_3^-$ as the counterion and more favorably lead to inner-sphere ion pairs, blocking the vacant coordination site and competing with monomer coordination and the formation of β-CH agostic species.[16] This inner-sphere coordination would reduce the overall catalytic activity, but would also lead to a lower impact of chain-transfer reactions and to higher MW polymers,[57] as observed with the activation of **C1** with $B(C_6F_5)_3$. This study suggests that the use of $B(C_6F_5)_3$ for Ni-catalyzed ethylene polymerization has a profound influence on the chain-propagation to access high MW polymers via an inner-sphere ion pair interaction.

DFT Study for Counter Ion Interaction. To validate the above proposition of a stronger inner-sphere interaction for the $ClB(C_6F_5)_3^-$ anion, a computational investigation was conducted. The DFT calculations aimed at elucidating the structural and energetic differences in the interaction of the cationic nickel catalyst with the $BArF^-$ and $ClB(C_6F_5)_3^-$ anions. The ligand was initially simplified to the unsubstituted pyridine-imine, NC_5H_4-2-CH=NH, and the PE chain was truncated to a propyl group, generated by insertion of an ethylene molecule into the Ni-CH_3 bond, for a full quantum mechanical (QM) approach. However, later calculations also addressed the system with the real ligand (**L1**) at the QM/MM level (Figure 5, Top). The geometry optimizations were conducted in the presence of a polarizable continuum with the permittivity of dichloromethane and thermal corrections were applied to obtain standard Gibbs energy values in condensed medium (298 K, 1 mol/L). The cation−anion interaction was investigated only for the most stable Ni−Pr isomer, namely the β-agostic complex with the propyl group *trans* to the pyridine ring (Figure S140). At the full QM level on the simplified system, for both anions, the addition with displacement of the β-agostic CH ligand is exoergic. The addition of ethylene lowers the Gibbs energy of the system by −12.8 kcal mol^{-1}, whereas the anion coordination lowers it by −13.2 kcal mol^{-1} for $ClB(C_6F_5)_3^-$ and −5.1 kcal mol^{-1} for $BArF^-$ (Figure 5, Bottom). The coordination site left open by dissociation of the propyl C−H function is saturated by interaction with a Cl lone pair for the former anion and an F lone pair for the latter one. The suitability of the QM/MM approach was first tested by reoptimizing handling the three noninteracting C_6H_3-3,5-$(CF_3)_2$ groups of the BArF anion at the molecular mechanics level, yielding comparable stabilization (−5.5 vs −5.1 kcal mol^{-1}) and metric parameters (Figure S141). The results of the QM/MM calculations for the model system with ligand **L1** are shown in Figure 5. Views of the optimized molecules are in Figure S143.

The greater stabilization associated with the $ClB(C_6F_5)_3^-$ coordination is obviously related to the greater donor power of the **Cl** lone pair in the B−Cl bond, relative to the F lone pair in the C−F bond of the $BArF^-$ anion. In the structure of the $[Ni(NC_5H_4CHNH)(Pr)]^+ClB(C_6F_5)_3^-$ adduct, the Ni−Cl distance (2.250 Å) is slightly longer than in the optimized $[Ni(NC_5H_4CHNH)(Pr)Cl]$ complex (2.225 Å, a lengthening by only 0.025 Å), but the B−Cl distance (2.255 Å) is much

https://doi.org/10.1021/acscatal.4c02708
ACS Catal. 2024, 14, 13136−13147

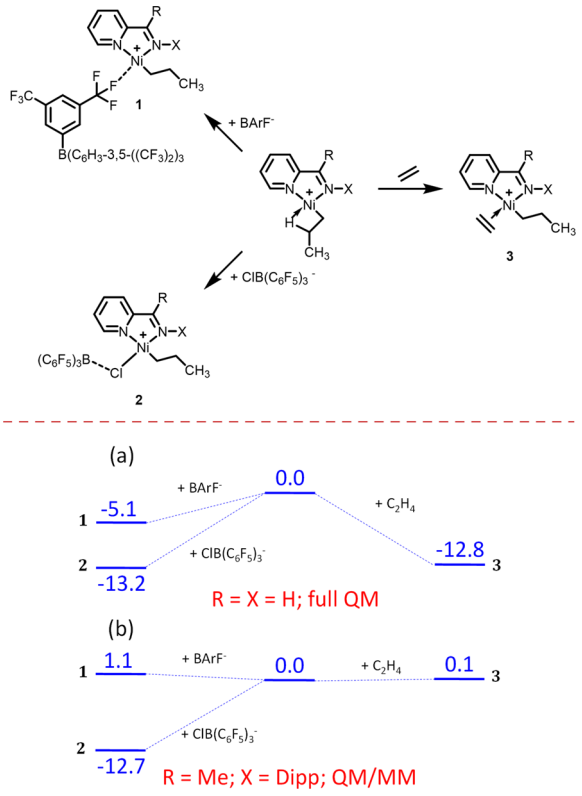

Figure 5. Cation−anion ion pair interaction with **C1**. Top: Interaction between the $[Ni(NC_5H_4CRNX)(Pr)]^+$ cation (center) and the $BArF^-$ and $ClB(C_6F_5)_3^-$ anions (left) and ethylene monomer (right). Bottom: Gibbs energy profile (values in kcal mol^{-1}) for the (a) simplified ligand (X = R = H) at the full QM level; (b) ligand **L1** (X = Dipp, R = Me) at the QM/MM level (the Dipp substituent in the cation, the three C_6F_5 groups in the Cl-BCF anion and the three noninteracting C_6H_3-3,5-$(CF_3)_2$ groups in the BArF anion were treated at the MM level).

longer than in the free $ClB(C_6F_5)_3^-$ anion (2.003 Å, a lengthening by 0.252 Å).[58] For the QM/MM calculation on $[Ni(NC_5H_4CMeNDipp)(Pr)]^+ClB(C_6F_5)_3^-$, the corresponding distances are 2.264 Å (Ni−Cl) and 2.695 vs 2.135 Å for B−Cl in the adduct and free $ClB(C_6F_5)_3^-$ anion, respectively (Figure S143). Furthermore, the B atom is pyramidalized (sum of the three CBC angles = 350.7° in the QM model, 353.2° in the QM/MM **L1** model) to a much lesser extent than in the free $ClB(C_6F_5)_3^-$ anion (QM: 340.8°; QM/MM: 341.0°), whereas the neutral $B(C_6F_5)_3$ Lewis acid has a planar B atom (360°). These structural parameters suggest that the Ni−Cl−B bonding is better considered as a weak dative interaction from the **Cl** ligand in the neutral $[Ni(NC_5H_4CHNH)(Pr)Cl]$ complex to the B atom in the $B(C_6F_5)_3$ Lewis acid (Ni−Cl → B), rather than as a NiCl−B dative interaction from the $ClB(C_6F_5)_3^-$ anion to the $[Ni(NC_5H_4CHNH)(Pr)]^+$ cation. The Gibbs energy of the $[Ni(NC_5H_4CHNH)(Pr)Cl]$ + $B(C_6F_5)_3$ system is −12.2 kcal mol^{-1} relative to the β-agostic $[Ni(NC_5H_4CHNH)(Pr)]^+$ cation + $ClB(C_6F_5)_3^-$ anion, namely only +1.0 kcal mol^{-1} relative to the inner-sphere ion pair (Figure S142). Thus, according to these calculations, the Lewis acid−base interaction between $[Ni(NC_5H_4CHNH)(Pr)Cl]$ and $B(C_6F_5)_3$ is weak but can furnish the β-agostic alkyl complex as a kinetically competent intermediate and then the ethylene adduct can form rather easily. In the structure of the inner-sphere $[Ni(NC_5H_4CRNX)(Pr)]^+BArF^-$ ion pairs (QM: X = R = H; QM/MM; R = Me, X = Dipp), the Ni−F distance is 2.082 (QM) or 2.091 (QM/MM) Å and the C−F distance of the Ni-coordinated CF bond is 1.432 (QM) or 1.429 (QM/MM) Å, whereas all other noninteracting CF bonds are a bit shorter (QM: 1.35−1.36 Å; QM/MM: 1.382−1.384 Å), attesting the non-negligible effect of the F → Ni interaction on the C−F bond. Comparison of the energetic parameters for the simplified system (full QM, Figure 5, Bottom a) and for the better **L1** model (QM/MM, Figure 5, Bottom b) suggests that the steric effect of the Dipp substituent plays an important role particularly on the monomer coordination and on the coordination of the bulkier $BArF^-$ anion, whereas it has a very minor destabilizing effect on the addition of the $ClB(C_6F_5)_3^-$ anion.

In conclusion, the $B(C_6F_5)_3$ Lewis acid is able to activate the Ni−Cl bond to remove the chloride ion from the nickel coordination sphere, but the cation interaction with $ClB(C_6F_5)_3^-$ competes efficiently with the ethylene coordination, whereas the $BArF^-$ anion has essentially no retardation effect. The inner-sphere $[Ni(NC_5H_4CMeNDipp)(Pr)]^+ClB(C_6F_5)_3^-$ ion pair, better described as a $[Ni(NC_5H_4CMeNDipp)(Pr)(Cl)]\cdots B(C_6F_5)_3$ Lewis acid−base adduct, is predicted to be the resting state of the propagation process, rather than the outer-sphere $[Ni(NC_5H_4CMeNDipp)(Pr)(C_2H_4)]^+ClB(C_6F_5)_3^-$ ion pair, and the energy span of the propagation process is greater, resulting in a slower polymerization.[58]

Ethylene Polymerization Study with C1−C8. Since $B(C_6F_5)_3$ has been found to be an exceptional activator for this system yielding higher MW materials, we sought to investigate the substituent effect using $B(C_6F_5)_3$ for all iminopyridyl complexes. Ethylene polymerizations were conducted at 20 °C with 400 psi of ethylene pressure, yielding the results

Table 2. Ethylene Polymerization of C1−C8 at 20 °C[a]

entry	catalyst	time (min)	yield (g)	productivity (kg mol^{-1}_{Ni} h)	TOF (10^3)(h^{-1})	B/1000C[b]	M_n[c] (kg mol^{-1})	$Đ$[c]	T_m[d] (°C)
1[e]	**C1**	10	2.4	2880	102.9	25	11.4	1.93	108.6
2	**C3**	10	1.7	1020	36.4	30	7.8	1.94	101.0
3	**C5**	10	1.6	960	34.3	37	11.7	1.97	99.7
4	**C7**	10	0.8	480	16.8	26	153.7	1.77	101.5
5[e]	**C2**	60	1.5	300	10.7	36	6.9	1.92	102.1
6	**C4**	60	0.9	90	3.2	49	23.8	1.75	112.0
7	**C6**	60	1.2	120	4.3	45	37.0	1.62	82.9
8	**C8**	180	0.5	167	0.6	42	71.3	2.06	91.5

[a]Conditions: 10 μmol of Ni catalyst, 10 equiv of $B(C_6F_5)_3$, 400 psi ethylene, 45 mL of toluene. [b]Determined by ^1H NMR in D_2-tetrachloroethane at 125 °C. [c]Determined by GPC in 1,2,4-trichlorobenzene at 160 °C using polystyrene calibration. [d]Determined by differential scanning calorimetry. [e]5 μmol of Ni. TOF = Turnover Frequency, M_n = Number-Average Molecular Weight, $Đ$ = Dispersity, T_m = Melting Temperature.

https://doi.org/10.1021/acscatal.4c02708
ACS Catal. 2024, 14, 13136−13147

Table 3. Ethylene/Polar Monomer Copolymerization of C7[a]

entry	monomer (M)	temp. (°C)	yield (g)	TOF (10^3)(h^{-1})	B/1000C[b]	M_n[c] (kg mol^{-1})	$Đ$[c]	incorp.[b] (mol %)	T_m[d] (°C)	T_g[d] (°C)
1[e]		40	3.2	11.4	57	111.6	1.71		68.7	−36.0
2	VTEoS [0.5]	40	0.8	0.7	52	66.3	1.60	3.1	56.2	−55.0
3[f]	VTEoS [0.5]	60	1.2	2.1	69	33.0	1.68	4.6	27.2	−64.7
4	VTEoS [1.0]	40	0.45	0.4	50	48.1	1.79	5.9	46.8	−63.6
5[g]	MA [0.1]	40	0.15	0.06	61	55.6	1.57	0.34	73.1	−39.2
6[g]	MA [0.1]	60	0.3	0.1	83	35.8	1.66	2.2	26.4	−51.9
7[g]	VAc [0.25]	60	0.5	0.2	78	53.3	1.65	0.26	46.9	−49.8

[a]Conditions: 20 μmol of **C7**, 1.2 equiv of AgBArF, 400 psi ethylene, 45 mL of toluene, 120 min. [b]Determined by ^{1}H NMR in D_2-tetrachloroethane at 125 °C. [c]Determined by GPC in 1,2,4-trichlorobenzene at 160 °C using polystyrene calibration. [d]Determined by differential scanning calorimetry. [e]10 μmol of **C7**, 60 min. [f]10 umol of **C7** [g]240 min. [M] = molar concentration, TOF = Turnover Frequency, M_n = Number-Average Molecular Weight, $Đ$ = Dispersity, T_m = Melting Temperature, VTEoS = vinyltriethoxysilane, MA = methyl acrylate, VAc = vinyl acetate.

Table 4. Ethylene Polymerization of C1 at 0−80 °C[a]

entry	temp (°C)	time (min)	yield (g)	productivity (kg mol^{-1}_{Ni} h)	TOF (10^3)(h^{-1})	M_n[b] (kg mol^{-1})	$Đ$[b]	T_m[c] (°C)	B/1000C[d]	branching distribution (%)[f] Me	Et	Pr	Bu	Am	Lg
1	0	30	1.1	440	15.7	65.1	1.65	127.8	5	100	0	0	0	0	0
2	20	10	2.4	2880	102.9	11.4	1.93	108.6	25	94.3	3.5	2.2	0	0	0
3	40	10	1.8	2160	77.1	3.7	1.66	64.4	56(46)[e]	80.0	4.7	2.9	2.6	2.1	7.6
4	60	10	2.2	2640	94.3	2.0	1.51	9.3	95(72)[e]	74.0	6.2	4.1	2.6	3.4	9.7
5	80	10	0.7	840	30.0	1.0	1.74	−23.6	127(81)[e]	66.4	7.5	4.5	2.8	6.6	12.1

[a]Conditions: 5 μmol of Ni catalyst, 10 equiv of $B(C_6F_5)_3$, 400 psi ethylene, 45 mL of toluene. [b]Determined by GPC in 1,2,4-trichlorobenzene at 160 °C using polystyrene calibration. [c]Determined by differential scanning calorimetry. [d]Determined by ^{1}H NMR in D_2-tetrachloroethane at 125 °C. [e]Branching density corrected for saturated end groups. [f]Determined by ^{13}C NMR in D_2-tetrachloroethane at 125 °C. Percentages of branch length determined from relative intensity ratios of methyl ($1B_1$, $1B_2$, $1B_3$), methylene ($2B_4$, $3B_5$) or methine (brB_{4+}) signals of the respective branch. TOF = Turnover Frequency, M_n = Number-Average Molecular Weight, $Đ$ = Dispersity, T_m = Melting Temperature, Me = Methyl, Et = Ethyl, Pr = Propyl, Bu = Butyl, Am = Amyl, Lg = Large.

summarized in Table 2. Complexes with the methyl group on the bridging carbon atom (**C1**, **C3**, **C5**, and **C7**) highlight the effect of increasing the steric bulk on the aryl imine moiety. No significant difference in MWs was observed for the polymers produced by **C1**, **C3** and **C5** (M_n = 11.4, 7.8, and 11.7 kg mol^{-1}), in line with the marginal increase of the calculated V_{Bur}%. Although the V_{Bur}% increases to only 47.6% in **C7**, the polymers produced have the highest MWs of the methyl bridging carbon series (M_n = 153.7 kg mol^{-1}) with lower dispersity ($Đ$ = 1.77) at 20 °C. This is over 10 times higher than any previously tested complex with a methyl-substituted carbon bridging and 5 times higher than similar catalysts activated with organoaluminum (Table 2, entry 4).[41] The data suggests that the benzosuberyl ligand provides a rigid steric environment that orients the aryl moiety closed to the metal center and further supports the hypothesis that higher MW materials can also be achieved with a more rigid ligand design.

Complexes with the phenyl group on the bridging carbon (**C2**, **C4**, **C6**, and **C8**) should increase the rotational restriction of the aryl imine substituents. **C2** exhibited low catalytic activity (TOF = 10,700 h^{-1}) and lower in MW (M_n = 6.9 kg mol^{-1}) compared with **C1**. Surprisingly, **C4** exhibited a completely different result and was able to produce PE with MW more than triple compared to **C3** (M_n = 23.8 kg mol^{-1}) (Table 2, entry 6). The polymerization results of **C4** supported our hypothesis that the phenyl substituent on the bridging carbon atom acts as a rotational barrier and is key for producing higher MW polymers. Like **C4**, **C6** produced much higher MW PE (M_n = 37.0 kg mol^{-1}) with lower dispersity (Table 2, entry 7) and further confirmed our hypothesis, where bulkier bridging carbon substituents can provide higher shielding to the metal center. As for **C2**, the isopropyl group is not bulky enough even with the phenyl group acting as a rotational barrier, thus resulting in low MW PEs. Synthetic challenges in preparing pure and isomer-free ligands, low complexation, and turnover yields, classified **C8** as a complex with undesirable properties. The data suggests that emphasis on the design of ligands with a rotational barrier provided by the bridging carbon atom substituent may be more effective at producing higher MW polymers.

Copolymerization. The copolymerization of ethylene with a small percent incorporation of polar monomers (2−5 mol %) can introduce functionalities that combine the high strength and durability of PE with improved chemical resistance, adhesion, polarity, and mechanical properties. Numerous Ni complexes have been reported for the copolymerization of ethylene with polar monomers, utilizing various ligands such as α-diimine, phosphine-sulfonate, salicylaldimine, and *N*-heterocyclic carbene, among others.[59] However, iminopyridine ligands have predominantly been reported for ethylene copolymerization in the form of Pd complexes, capable of producing copolymers with both high molecular weights and percentages of methyl acrylate (MA) and acrylic acid incorporation.[40,50,60,61] In comparison, dihalide iminopyridyl Ni^{II} complexes can only produce low MW copolymers with moderate MA incorporation (4.8 kg mol^{-1} with 2.4 mol %).[43] We selected **C7** for ethylene/polar monomer copolymerization as the complex can produce high MW PE at ambient conditions. Interestingly, **C7** produced ethylene/MA copolymers (Table 3, entries 5 and 6) with higher MW (35.8 kg mol^{-1}) and 2.2 mol % incorporation. Additionally, we tested vinyltriethoxysilane (VTEoS) and vinyl acetate (VAc), which have never been reported as comonomers for iminopyridyl Ni^{II} complexes. With 0.5 M VTEoS loading, **C7** produced copolymer with moderate MW (66.3 kg mol^{-1}) and 3 mol % incorporation (Table 3, entry 2). Increasing the loading to

https://doi.org/10.1021/acscatal.4c02708
ACS Catal. 2024, 14, 13136−13147

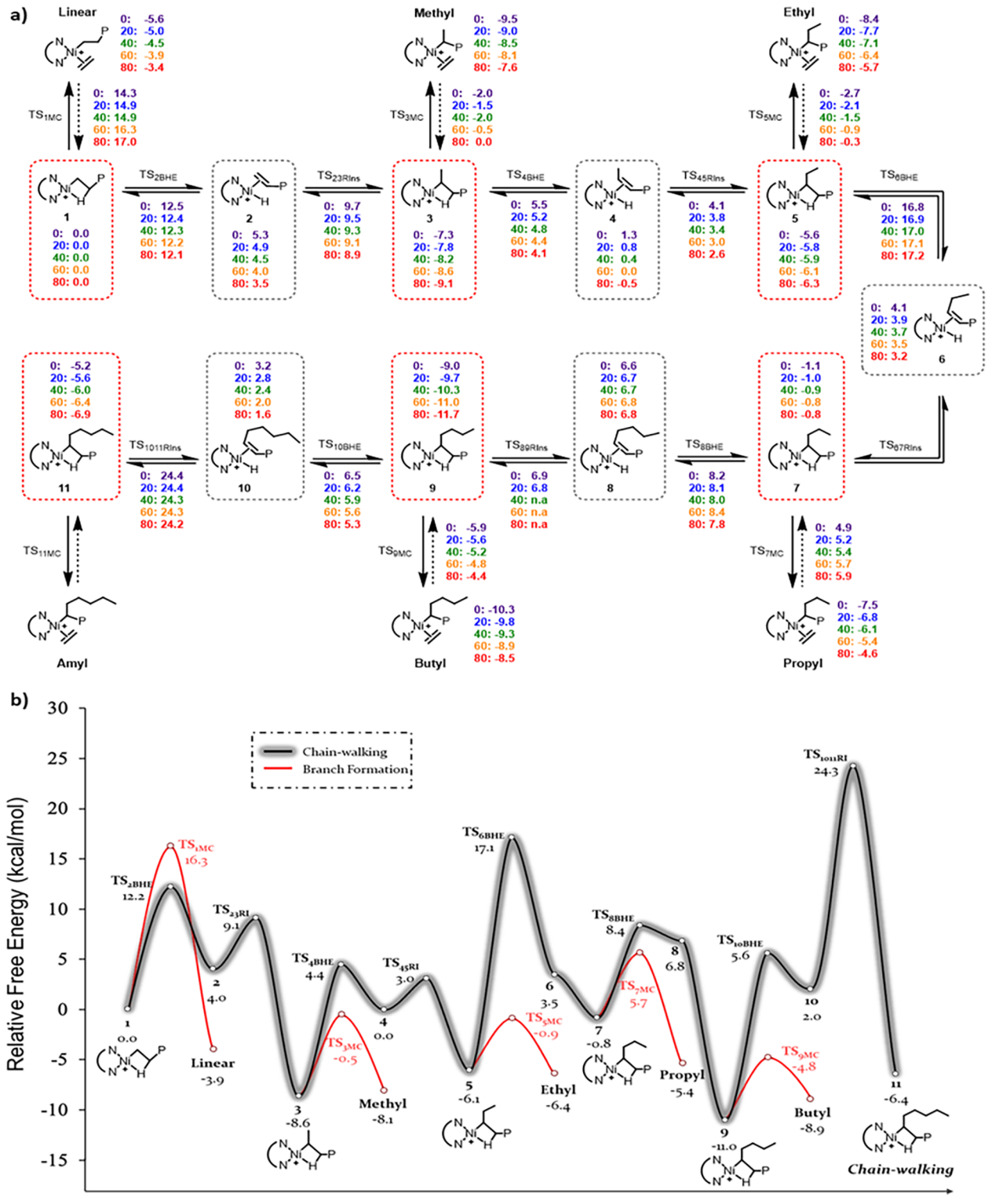

Figure 6. Mechanism and Gibbs energy diagram for chain-walking mechanism. (a) Chain-walking and propagation mechanism with Gibbs energies for reaction temperatures from 0 to 80 °C. (b) Free energy diagram for chain-walking and propagation for **C1** calculated from DFT at 60 °C. TS: transition state; BHE: β-hydride elimination; RI: reinsertion; MC: monomer coordination.

1.0 M nearly doubled the mol % incorporation with a slight decrease in MW to 48.1 kg mol^{-1} (Table 3, entry 4). For copolymerization with VAc, **C7** produced copolymers with MWs of 53.3 kg mol^{-1} and incorporation of 0.26 mol % (Table 3, entry 7).

Branching Density and Distribution. To confirm the thermal stability of the carbyl complexes, **C1** was assessed at reaction temperatures ranging from 0 to 80 °C. The complex is still highly active in polymerization reactions up to 60 °C, which is indicative of good thermal stability (TOF = 94,300 h^{-1}). However, at 80 °C, the activity dramatically decreases to 30,000 h^{-1} which suggests catalyst degradation. We observed that the MW of PEs from C1 is highly dependent on the reaction temperature. With decreasing temperatures, the MW

https://doi.org/10.1021/acscatal.4c02708
ACS Catal. 2024, 14, 13136−13147

of PEs increased to 65.1 kg mol^{-1} at 0 °C (Table 4, **entry 1**). Only oligomers were generated at temperatures above 40 °C (Table 4, **entry 4**, **5**). A similar trend was observed in the iminopyridyl Ni^{II} catalysts **C2**−**C7**, with **C4** producing high MW polymers at 0 °C (M_n = 164.6 kg mol^{-1}) and 5.6 kg mol^{-1} at 60 °C with the addition of the rotational barrier provided by the bridging carbon (Table S1).

Surprisingly, the branching density of PEs obtained from **C1** exhibited a linear relationship with respect to the reaction temperature under high pressure conditions where chain-walking should be suppressed (Figure S1).[62] ^{1}H NMR and differential scanning calorimetry (DSC) showed that the PEs obtained from **C1** at 0 °C had 5 branches/1000 carbon atoms and a T_m of 127.8 °C, classifying the polymer as HDPE. At 20 °C, the branching density increased to 25 branches/1000 carbon atoms and a decrease in T_m to 108.6 °C, characteristic of LLDPE. A wax-like LLDPE was obtained at 40 °C, with a branching density of 56 branches/1000 carbon atoms and a T_m of 64.4 °C. An LDPE-like material was generated at 60 °C with a branching density of 95 branches/1000 carbon atoms and a T_m of 9.3 °C, and an oligomeric oil was formed at 80 °C (Table 3, entries 1−5). A similar linear branching trend was observed with complexes **C2**−**C7** in the same reaction temperature range. For example, **C4** ranged from 18 branches/1000 carbon atoms at 0 °C to 104 branches/1000 carbon atoms at 60 °C. We suggest that the unique control of the branching density exhibited by the carbyl Ni^{II} complexes is influenced by the iminopyridine ligand in combination with the inner-sphere organoboron/Ni ion pair and reaction temperature. In comparison to "half-sandwich" iminopyridyl Ni^{II} complexes, their branching density is limited to a range of 79 to 125 branches/1000 carbon atoms at 25 and 70 °C.[63] In summary, a single catalyst can produce several types of PEs with broad branching densities. This versatility is achieved without the need for expensive comonomers, making it highly desirable in polyolefin syntheses and processes. We point out that it is unusual for these complexes to produce a wide variety of PE at high pressures, where chain-walking should be retarded.

The ability to produce a wide range of branching densities resulted in the production of diverse materials and prompted further investigation into their unique microstructures. The material properties of the PE suggest a branching microstructure commonly achieved through α-olefin copolymerization, which introduces short-chain branches (SCBs). It has been understood that the controlled incorporation of SCBs, where the branch length is 5 carbon atoms or less, can dramatically impact the mechanical properties of PE.[64] Therefore, the analysis of the branching microstructure of polymers produced by **C1** under high ethylene pressure was conducted using quantitative ^{13}C NMR spectroscopy (Figures S58−S63) and is included in Table 4.[65,66]

At 0 °C, only methyl branches are observed. Increasing the temperature to 20 °C induces the incorporation of ethyl, and propyl branches. Additional ethyl and propyl branches were observed in the polymer at 40 °C, with butyl, amyl, and long-chain branches (LCBs) being detected. At 60 and 80 °C, incorporation of short- and long-chain branches gradually increased at the expense of methyl branches. Current imine-chelated Ni^{II} complexes must utilize low pressure conditions and/or elaborate ligand designs to promote chain-walking and tailor the polymer microstructure.[67,68] However, this strategy is not effective as the incorporation of SCBs is negligible. Since our system produces SCBs under high pressure conditions and is not supported by established mechanistic understandings, we sought to further investigate the underlying chain-walking mechanism through computational studies. Therefore, additional DFT calculations were conducted for **C1** with respect to temperatures ranging from 0 to 80 °C.

DFT Calculations for Chain-Walking Mechanism. The polymerization is modeled from the β-CH agostic species **1**, the resting state, with a propagating polymer chain (Figure S144). The metal can either chain-walk across the polymer or produce branches at key intermediates **1**, **3**, **5**, **7**, **9**, and **11** via ethylene coordination (Figure 6a). The Gibbs energy profile at 60 °C serves as a representative data set to discuss the branching distribution and free energies (Figure 6b). The remaining Gibbs energy profiles are included as Figures S145−S148. From these profiles, it can be determined that higher reaction temperatures enable the gradual incorporation of longer branches due to increased thermal energy (k_bT), which is consistent with the branching distribution reported in Table 3. The first pathway is a coordination/insertion of ethylene to produce a linear polymer (**Linear**), where monomer coordination must overcome an energy barrier (**TS$_{1MC}$**) of 16.3 kcal mol^{-1} and is exergonic by 3.9 kcal mol^{-1}. Alternatively, the agostic species **1** can undergo β-hydride elimination (**TS$_{2BHE}$**) to form the olefin π-complex **2**, with an energy barrier of 12.2 kcal mol^{-1}. This complex can then undergo 2,1-reinsertion (**TS$_{23RI}$**), with an energy barrier of 5.1 kcal mol^{-1}, generating in the new β-CH agostic species **3**, a process exergonic by −12.6 kcal mol^{-1} and more favorable than direct ethylene coordination−insertion by 4.7 kcal mol^{-1}. Species 3 can again either undergo monomer coordination (**TS$_{3MC}$**) with an energy barrier of 8.1 kcal mol^{-1} to produce a methyl branch (**Methyl**) or β-hydride elimination (**TS$_{4BHE}$**) for further chain-walking. However, with a 13.0 kcal mol^{-1} energy barrier for chain-walking, methyl branch formation is more favorable, and is the predominant branch experimentally observed at all temperatures.

Once the agostic species **3** crosses the barrier **TS$_{4BHE}$**, it forms olefin π-complex 4, which can undergo 3,2-reinsertion (**TS$_{45RI}$**) with a minimal barrier of only 3.0 kcal mol^{-1}, resulting in the β-CH agostic complex **5** in an exergonic step (−6.1 kcal mol^{-1}). Following the formation of complex **5**, β-elimination must overcome a barrier of 23.2 kcal mol^{-1} (**TS$_{6BHE}$**). In contrast, the barrier for ethylene insertion to produce ethyl branched (**Ethyl**) is significantly lower at 5.2 kcal mol^{-1} (**TS$_{5MC}$**) and occurs in a mildly exergonic step (−0.3 kcal mol^{-1}). After β-elimination from complex **5**, the subsequent reinsertion step is barrierless for all reaction temperatures, leading to the spontaneous formation of β-CH agostic complex **7**. The overall chain-walking step from **5** to **7** is endergonic by 5.3 kcal mol^{-1}. The large energy barrier from **5** to **7** confirms the preference for higher precent incorporation of ethyl branches over propyl branches across all reaction temperatures. From complex **7**, the barrier for propyl branch formation (**TS$_{7MC}$**) is 6.5 kcal mol^{-1}, which is slightly lower than the barrier of 9.2 kcal mol^{-1} (**TS$_{8BHE}$**) for β-elimination leading to complex **8**, which then spontaneously converts to complex **9** at temperatures above 40 °C. Following this, β-elimination to olefin π-complex **10**, followed by the 6,5-reinsertion to β-CH agostic complex **11** is the precursor to form amyl branches. The β-elimination step is endergonic by 13.0 kcal mol^{-1} with an activation barrier of 16.6 kcal mol^{-1} (**TS$_{10BHE}$**), yet the reinsertion step is exergonic and

https://doi.org/10.1021/acscatal.4c02708
ACS Catal. 2024, 14, 13136−13147

thermodynamically favorable. Although the high activation barrier value of 22.3 kcal mol^{-1} for reinsertion (TS_{1011RI}) suggests a low amount of amyl branches, reactions above 60 °C have greater percent incorporation (Table 3, entries 3−5) due to the increase in the total thermal energy in the system. This increase in thermal energy subsequently also produces larger chain branches (**Lg**).

CONCLUSIONS

In this work, benchtop-stable iminopyridyl Ni(II) complexes were prepared bearing an *o*-tolyl carbyl substituent which allows for the study of the effect that ion pairs have on olefin polymerization. Early transition metal complexes demonstrate the importance of the counterion in controlling polyolefin microstructures, but the influence and impact of counterion effects in late transition complexes, specifically for [*N*,*N*]-chelated Ni^{II} complexes have been largely unexplored, due to the absence of a suitable thermodynamically stable complexes. We demonstrated that the well-defined, inner-sphere $ClB(C_6F_5)_3^-$ counterion provides an altered resting state for propagation, inhibiting key intermediates responsible for chain-walking and chain-termination, thus producing higher MW PE with controlled short-chain branching distributions. This branching control provided materials with properties comparable to HDPE, LLDPE, and LDPE. Additionally, we demonstrated that the substituents on the bridging carbon can act as a rotational barrier imposing more axial bulk around the metal center which favors chain-propagation. This emphasizes the importance of substituent placement on the bridging carbon moiety, instead of the more traditional ligand design focusing on the aryl imine. We anticipate that this study will invigorate the exploration of a broader scope of activators and inner-sphere counterions with the extensive iminopyridine or related diimine ligand catalog for the synthesis of polyolefins with tailored branching characteristics and properties.

ASSOCIATED CONTENT

Supporting Information

The Supporting Information is available free of charge at https://pubs.acs.org/doi/10.1021/acscatal.4c02708.

Experimental procedures, methods, computation, and characterization of compounds (PDF)
HR-C1 (CIF)
HR-C3 (CIF)
HR-C4 (CIF)
HR-C5 (CIF)
HR-C7 (CIF)
HR-C8 (CIF)

AUTHOR INFORMATION

Corresponding Authors

Rinaldo Poli − *CNRS, LCC (Laboratoire de Chimie de Coordination), UPS, INPT, Université de Toulouse, 31077 Toulouse Cedex 4, France; Institut Universitaire de France, 75231 Paris, France;* orcid.org/0000-0002-5220-2515; Email: rinaldo.poli@lcc-toulouse.fr

Lars C. Grabow − *Department of Chemical and Biomolecular Engineering, University of Houston, Houston, Texas 77204, United States;* orcid.org/0000-0002-7766-8856; Email: garbow@uh.edu

Eva Harth − *Department of Chemistry, Center of Excellence in Polymer Chemistry (CPEC), University of Houston, Houston, Texas 77004, United States;* orcid.org/0000-0001-5553-0365; Email: harth@uh.edu

Authors

Hasaan S. Rauf − *Department of Chemistry, Center of Excellence in Polymer Chemistry (CPEC), University of Houston, Houston, Texas 77004, United States*

Yu-Sheng Liu − *Department of Chemistry, Center of Excellence in Polymer Chemistry (CPEC), University of Houston, Houston, Texas 77004, United States*

Muhammad Arslan − *Department of Chemistry, Center of Excellence in Polymer Chemistry (CPEC), University of Houston, Houston, Texas 77004, United States;* orcid.org/0009-0000-5481-0568

Surya Pratap S. Solanki − *Department of Chemical and Biomolecular Engineering, University of Houston, Houston, Texas 77204, United States;* orcid.org/0000-0003-1921-0983

Eric Deydier − *CNRS, LCC (Laboratoire de Chimie de Coordination), UPS, INPT, Université de Toulouse, 31077 Toulouse Cedex 4, France*

Complete contact information is available at: https://pubs.acs.org/10.1021/acscatal.4c02708

Author Contributions

H.S.R. and Y.-S.L. conceived the project. H.S.R. and Y.-S.L. performed experimental studies including catalyst preparation and characterization polymer synthesis and analysis. M.A. supported experimental studies, catalyst preparation, polymerization studies, and analysis. H.S.R., Y.-S.L., and E.H. drafted the initial manuscript. H.S.R., Y.-S.L., and E.H. designed and edited figures. H.S.R., Y.-S.L., M.A., S.S.S., L.C.G., R.P., and E.H. edited and revised the text. E.D. and R.P. conducted DFT simulations for the counterion study and made the respective figures. S.S.S. and L.C.G. performed DFT simulations for the chain-walking mechanism and made the respective figures. L.C.G., R.P., and E.H. supervised the study. The manuscript was written through contributions of all authors.

Notes

The authors declare no competing financial interest.

ACKNOWLEDGMENTS

The authors H.S.R., Y.-S.L., M.A., and E.H. thank the Robert A. Welch Foundation for funding (H-E-0041 and E-2066-202110327) through the Center of Excellence in Polymer Chemistry and acknowledge the National Science Foundation (CHEM-2108576) for supporting parts of this work. R.P. and E.D. thank the CALMIP Mesocenter of the University of Toulouse for the allocation of computational resources. S.S.S. and L.C.G. were supported by NSF EFRI Award # 2029359, and acknowledge the use of the Carya, Opuntia, and Sabine Clusters and the advanced support from the Research Computing Data Core at the University of Houston. Jacobo Strong is acknowledged for his contributions to early $B(C_6F_5)_3$ activation studies, insightful and engaging discussions, and for a critical review and editing of the manuscript.

REFERENCES

(1) Hustad, P. D. Frontiers in Olefin Polymerization: Reinventing the World's Most Common Synthetic Polymers. *Science* **2009**, *325* (5941), 704−707.

(2) Mülhaupt, R. Green Polymer Chemistry and Bio-based Plastics: Dreams and Reality. *Macromol. Chem. Phys.* **2013**, *214* (2), 159−174.

(3) Stürzel, M.; Mihan, S.; Mülhaupt, R. From Multisite Polymerization Catalysis to Sustainable Materials and All-Polyolefin Composites. *Chem. Rev.* **2016**, *116* (3), 1398−1433.
(4) Sauter, D. W.; Taoufik, M.; Boisson, C. Polyolefins, a Success Story. *Polymers* **2017**, *9* (6), 185.
(5) Zhang, Y.; Zhang, Y.; Hu, X.; Wang, C.; Jian, Z. Advances on Controlled Chain Walking and Suppression of Chain Transfer in Catalytic Olefin Polymerization. *ACS Catal.* **2022**, *12* (22), 14304−14320.
(6) Chen, A.; Ma, Z.; Pan, Y.; Chen, M.; Zou, C. Cocatalyst Effect in Transition Metal Catalyzed Ethylene Polymerization and Copolymerization. *ChemCatChem.* **2022**, *14* (19), No. e202200578.
(7) Li, L.; Stern, C. L.; Marks, T. J. Bis(Pentafluorophenyl)(2-perfluorobiphenylyl)borane. A New Perfluoroarylborane Cocatalyst for Single-Site Olefin Polymerization. *Organometallics* **2000**, *19* (17), 3332−3337.
(8) Urciuoli, G.; Zaccaria, F.; Zuccaccia, C.; Cipullo, R.; Budzelaar, P. H. M.; Vittoria, A.; Ehm, C.; Macchioni, A.; Busico, V. Cocatalyst effects in Hf-catalysed olefin polymerization: taking well-defined Al−alkyl borate salts into account. *Dalton Trans.* **2024**, *53* (5), 2286−2293.
(9) Wang, Q.; Zhang, Z.; Zou, C.; Chen, C. A general cocatalyst strategy for performance enhancement in nickel catalyzed ethylene (co)polymerization. *Chin. Chem. Lett.* **2022**, *33* (9), 4363−4366.
(10) Chen, E. Y.-X.; Marks, T. J. Cocatalysts for Metal-Catalyzed Olefin Polymerization: Activators, Activation Processes, and Structure−Activity Relationships. *Chem. Rev.* **2000**, *100* (4), 1391−1434.
(11) Chen, Y.-X.; Metz, M. V.; Li, L.; Stern, C. L.; Marks, T. J. Sterically Encumbered (Perfluoroaryl) Borane and Aluminate Cocatalysts for Tuning Cation−Anion Ion Pair Structure and Reactivity in Metallocene Polymerization Processes. A Synthetic, Structural, and Polymerization Study. *J. Am. Chem. Soc.* **1998**, *120* (25), 6287−6305.
(12) Mohammed, M.; Nele, M.; Al-Humydi, A.; Xin, S.; Stapleton, R. A.; Collins, S. Counterion Effects on Propylene Polymerization Using Two-State ansa-Metallocene Complexes. *J. Am. Chem. Soc.* **2003**, *125* (26), 7930−7941.
(13) Li, H.; Li, L.; Marks, T. J.; Liable-Sands, L.; Rheingold, A. L. Catalyst/Cocatalyst Nuclearity Effects in Single-Site Olefin Polymerization. Significantly Enhanced 1-Octene and Isobutene Comonomer Enchainment in Ethylene Polymerizations Mediated by Binuclear Catalysts and Cocatalysts. *J. Am. Chem. Soc.* **2003**, *125* (36), 10788−10789.
(14) Zaccaria, F.; Sian, L.; Zuccaccia, C.; Macchioni, A. Chapter One - Ion pairing in transition metal catalyzed olefin polymerization. In *Adv. Organomet. Chem.*; Pérez, P. J. Ed.; Academic Press: 2020; Vol. *73*, pp 1−78.
(15) Chien, J. C.; Song, W.; Rausch, M. D. Effect of counterion structure on zirconocenium catalysis of olefin polymerization. *Macromolecules* **1993**, *26* (12), 3239−3240.
(16) Chen, M.-C.; Roberts, J. A. S.; Marks, T. J. Marked Counteranion Effects on Single-Site Olefin Polymerization Processes. Correlations of Ion Pair Structure and Dynamics with Polymerization Activity, Chain Transfer, and Syndioselectivity. *J. Am. Chem. Soc.* **2004**, *126* (14), 4605−4625.
(17) Johnson, L. K.; Killian, C. M.; Brookhart, M. New Pd(II)- and Ni(II)-Based Catalysts for Polymerization of Ethylene and.alpha.-Olefins. *J. Am. Chem. Soc.* **1995**, *117* (23), 6414−6415.
(18) Ittel, S. D.; Johnson, L. K.; Brookhart, M. Late-Metal Catalysts for Ethylene Homo- and Copolymerization. *Chem. Rev.* **2000**, *100* (4), 1169−1204.
(19) Schleis, T.; Spaniol, T. P.; Okuda, J.; Heinemann, J.; Mülhaupt, R. Ethylene polymerization catalysts based on nickel(II) 1,4-diazadiene complexes: the influence of the 1,4-diazadiene backbone substituents on structure and reactivity1Dedicated to Professor Akira Nakamura with best personal wishes.1. *J. Organomet. Chem.* **1998**, *569* (1), 159−167.
(20) Souther, K. D.; Leone, A. K.; Vitek, A. K.; Palermo, E. F.; LaPointe, A. M.; Coates, G. W.; Zimmerman, P. M.; McNeil, A. J. Trials and tribulations of designing multitasking catalysts for olefin/thiophene block copolymerizations. *J. Polym. Sci., Part A: Polym. Chem.* **2018**, *56* (1), 132−137.
(21) Xu, M.; Liu, Y.; Pang, W.; Pan, Y.; Chen, M.; Zou, C.; Tan, C. Cocatalyst effects in α-diimine nickel catalyzed ethylene polymerization. *Polymer* **2022**, *255*, No. 125116.
(22) Svoboda, M.; Dieck, H. t. Diazadien-nickel-alkyle. *J. Organomet. Chem.* **1980**, *191* (1), 321−328.
(23) Cámpora, J.; del Mar Conejo, M. a.; Mereiter, K.; Palma, P.; Pérez, C.; Reyes, M. L.; Ruiz, C. Synthesis of dialkyl, diaryl and metallacyclic complexes of Ni and Pd containing pyridine, α-diimines and other nitrogen ligands: Crystal structures of the complexes cis-NiR2py2 (R = benzyl, mesityl). *J. Organomet. Chem.* **2003**, *683* (1), 220−239.
(24) De Souza, R.-F.; Mauler, R. S.; Simon, L. C.; Nunes, F. F.; Vescia, D. V. S.; Cavagnolli, A. [η3-methallyl-nickel-dad]PF6 complex: new catalyst precursor for ethylene polymerization. *Macromol. Rapid Commun.* **1997**, *18* (9), 795−800.
(25) Johnson, L. K.; McLain, S. J.; Sweetman, K. J.; Wang, Y.; Bennett, A. M. A.; Wang, L.; McCord, E. F.; Lonkin, A.; Ittel, S. D.; Radzewich, C. E. WO 2003044066, 2003.
(26) Negureanu, L.; Hall, R. W.; Butler, L. G.; Simeral, L. A. Methyaluminoxane (MAO) Polymerization Mechanism and Kinetic Model from Ab Initio Molecular Dynamics and Electronic Structure Calculations. *J. Am. Chem. Soc.* **2006**, *128* (51), 16816−16826.
(27) Bonnet, M. C.; Dahan, F.; Ecke, A.; Keim, W.; Schulz, R. P.; Tkatchenko, I. Synthesis of cationic and neutral methallyl nickel complexes and applications in ethene oligomerisation. *J. Chem. Soc., Chem. Commun.* **1994**, *5*, 615−616.
(28) Wang, C.; Friedrich, S.; Younkin, T. R.; Li, R. T.; Grubbs, R. H.; Bansleben, D. A.; Day, M. W. Neutral Nickel(II)-Based Catalysts for Ethylene Polymerization. *Organometallics* **1998**, *17* (15), 3149−3151.
(29) Liang, T.; Goudari, S. B.; Chen, C. A simple and versatile nickel platform for the generation of branched high molecular weight polyolefins. *Nat. Commun.* **2020**, *11* (1), 372.
(30) Schiebel, E.; Voccia, M.; Falivene, L.; Caporaso, L.; Mecking, S. The Impact of Charge in a Ni(II) Polymerization Catalyst. *ACS Catal.* **2021**, *11* (9), 5358−5368.
(31) Shields, B. J.; Kudisch, B.; Scholes, G. D.; Doyle, A. G. Long-Lived Charge-Transfer States of Nickel(II) Aryl Halide Complexes Facilitate Bimolecular Photoinduced Electron Transfer. *J. Am. Chem. Soc.* **2018**, *140* (8), 3035−3039.
(32) Biewer, C.; Hamacher, C.; Kaiser, A.; Vogt, N.; Sandleben, A.; Chin, M. T.; Yu, S.; Vicic, D. A.; Klein, A. Unsymmetrical N-Aryl-1-(pyridin-2-yl)methanimine Ligands in Organonickel(II) Complexes: More Than a Blend of 2,2′-Bipyridine and N,N-Diaryl-α-diimines? *Inorg. Chem.* **2016**, *55* (24), 12716−12727.
(33) Laine, T. V.; Lappalainen, K.; Liimatta, J.; Aitola, E.; Löfgren, B.; Leskelä, M. Polymerization of ethylene with new diimine complexes of late transition metals. *Macromol. Rapid Commun.* **1999**, *20* (9), 487−491.
(34) Sun, W.-H.; Song, S.; Li, B.; Redshaw, C.; Hao, X.; Li, Y.-S.; Wang, F. Ethylene polymerization by 2-iminopyridylnickel halide complexes: synthesis, characterization and catalytic influence of the benzhydryl group. *Dalton Transactions* **2012**, *41* (39), 11999−12010.
(35) Yue, E.; Zhang, L.; Xing, Q.; Cao, X.-P.; Hao, X.; Redshaw, C.; Sun, W.-H. 2-(1-(2-Benzhydrylnaphthylimino)ethyl)pyridylnickel halides: synthesis, characterization, and ethylene polymerization behavior. *Dalton Transactions* **2014**, *43* (2), 423−431.
(36) Wang, F.; Chen, C. A continuing legend: the Brookhart-type α-diimine nickel and palladium catalysts. *Polym. Chem-Uk* **2019**, *10* (19), 2354−2369.
(37) Chen, Z.; Allen, K. E.; White, P. S.; Daugulis, O.; Brookhart, M. Synthesis of Branched Polyethylene with "Half-Sandwich" Pyridine-Imine Nickel Complexes. *Organometallics* **2016**, *35* (11), 1756−1760.
(38) Lu, W.; Liao, Y.; Dai, S. Facile access to ultra-highly branched polyethylenes using hybrid "sandwich" Ni(II) and Pd(II) catalysts. *J. Catal.* **2022**, *411*, 54−61.

https://doi.org/10.1021/acscatal.4c02708
ACS Catal. 2024, 14, 13136−13147

(39) Ge, Y.; Cai, Q.; Wang, Y.; Gao, J.; Chi, Y.; Dai, S. Synthesis of High-Molecular-Weight Branched Polyethylene Using a Hybrid "Sandwich" Pyridine-Imine Ni(II). *Catalyst. Front. Chem.* **2022**, *10*, No. 886888.
(40) Liao, Y.-D.; Cai, Q.; Dai, S.-Y. Synthesis of High Molecular Weight Polyethylene and E-MA Copolymers Using Iminopyridine Ni(II) and Pd(II) Complexes Containing a Flexible Backbone and Rigid Axial Substituents. *Chin. J. Polym. Sci.* **2023**, *41* (2), 233−239.
(41) Peng, H.; Li, S.; Li, G.; Dai, S.; Ji, M.; Liu, Z.; Guo, L. Rotation-restricted strategy to synthesize high molecular weight polyethylene using iminopyridyl nickel and palladium catalyst. *Appl. Organomet. Chem.* **2021**, *35* (3), No. e6140.
(42) D'Auria, I.; Milione, S.; Caruso, T.; Balducci, G.; Pellecchia, C. Synthesis of hyperbranched low molecular weight polyethylene oils by an iminopyridine nickel(ii) catalyst. *Polym. Chem.* **2017**, *8* (41), 6443−6454.
(43) D'Auria, I.; Saki, Z.; Pellecchia, C. Iminopyridine Ni(II) Catalysts Affording Oily Hyperbranched Ethylene Oligomers and/or Crystalline Polyethylenes Depending on the Reaction Conditions: Possible Role of In Situ Catalyst Structure Modifications. *Macromolecules* **2021**, *1* (2), 121−129.
(44) Mahmood, Q.; Li, X.; Qin, L.; Wang, L.; Sun, W.-H. Structural evolution of iminopyridine support for nickel/palladium catalysts in ethylene (oligo)polymerization. *Dalton Trans.* **2022**, *51* (38), 14375−14407.
(45) Laine, T. V.; Piironen, U.; Lappalainen, K.; Klinga, M.; Aitola, E.; Leskelä, M. Pyridinylimine-based nickel(II) and palladium(II) complexes: preparation, structural characterization and use as alkene polymerization catalysts. *J. Organomet. Chem.* **2000**, *606* (2), 112−124.
(46) Mogheiseh, M.; Zohuri, G. H.; Khoshsefat, M. Synthesis of LDPE Using Pyridineimine-Based Nickel (II) Bromide Complexes: Effect of Catalyst Bulkiness on Thermal, Structural, and Morphological Properties. *Macromol. React. Eng.* **2018**, *12* (5), No. 1800006.
(47) Lovett, D. M.; Thierer, L. M.; Santos, E. E. P.; Hardie, R. L.; Dougherty, W. G.; Piro, N. A.; Kassel, W. S.; Cromer, B. M.; Coughlin, E. B.; Zubris, D. L. Structural analysis of imino- and amino-pyridine ligands for Ni(II):Precatalysts for the polymerization of ethylene. *J. Organomet. Chem.* **2018**, *863*, 44−53.
(48) Lindley, B. M.; Wolczanski, P. T.; Cundari, T. R.; Lobkovsky, E. B. First-Row Transition Metal and Lithium Pyridine-ene-amide Complexes Exhibiting N- and C-Isomers and Ligand-Based Activation of Benzylic C−H Bonds. *Organometallics* **2015**, *34* (19), 4656−4668.
(49) Li, S.; Lu, Z.; Fan, W.; Dai, S. Efficient incorporation of a polar comonomer for direct synthesis of hyperbranched polar functional ethylene oligomers. *New J. Chem.* **2021**, *45* (8), 4024−4031.
(50) Li, S.; Dai, S. Highly efficient incorporation of polar comonomers in copolymerizations with ethylene using iminopyridyl palladium system. *J. Catal.* **2021**, *393*, 51−59.
(51) Falivene, L.; Cao, Z.; Petta, A.; Serra, L.; Poater, A.; Oliva, R.; Scarano, V.; Cavallo, L. Towards the online computer-aided design of catalytic pockets. *Nat. Chem.* **2019**, *11* (10), 872−879.
(52) Hayashi, Y.; Rohde, J. J.; Corey, E. J. A Novel Chiral Super-Lewis Acidic Catalyst for Enantioselective Synthesis. *J. Am. Chem. Soc.* **1996**, *118* (23), 5502−5503.
(53) Chen, Z.; Leatherman, M. D.; Daugulis, O.; Brookhart, M. Nickel-Catalyzed Copolymerization of Ethylene and Vinyltrialkoxysilanes: Catalytic Production of Cross-Linkable Polyethylene and Elucidation of the Chain-Growth Mechanism. *J. Am. Chem. Soc.* **2017**, *139* (44), 16013−16022.
(54) Normand, A. T.; Richard, P.; Balan, C.; Daniliuc, C. G.; Kehr, G.; Erker, G.; Le Gendre, P. Synthetic Endeavors toward Titanium Based Frustrated Lewis Pairs with Controlled Electronic and Steric Properties. *Organometallics* **2015**, *34* (10), 2000−2011.
(55) Punzalan, E.; Froese, R. D.; Zimmerman, P. M. Revealing the Interactions between the Flexible Polymer and Counteranion during Propagation and Termination for Olefin Polymerization with the Ti(IV) Constrained Geometry Catalyst. *Organometallics* **2023**, *42* (22), 3236−3248.
(56) Macchioni, A. Ion Pairing in Transition-Metal Organometallic Chemistry. *Chem. Rev.* **2005**, *105* (6), 2039−2074.
(57) Bochmann, M.; Cannon, R. D.; Song, F. Kinetic and mechanism of alkene polymerization. *Kinet. Catal.* **2006**, *47* (2), 160−169.
(58) Lassahn, P.-G.; Lozan, V.; Wu, B.; Weller, A. S.; Janiak, C. Dihalogeno(diphosphane)metal(ii) complexes (metal = Co, Ni, Pd) as pre-catalysts for the vinyl/addition polymerization of norbornene − elucidation of the activation process with B(C6F5)3/AlEt3 or Ag[closo-1-CB11H12] and evidence for the in situ formation of "naked" Pd2+ as a highly active species. *Dalton Trans.* **2003**, *23*, 4437−4450.
(59) Zhang, R.; Gao, R.; Gou, Q.; Lai, J.; Li, X. Recent Advances in the Copolymerization of Ethylene with Polar Comonomers by Nickel Catalysts. *Polymers* **2022**, *14* (18), 3809.
(60) Ge, Y.; Li, S.; Wang, H.; Dai, S. Synthesis of Branched Polyethylene and Ethylene-MA Copolymers Using Unsymmetrical Iminopyridyl Nickel and Palladium Complexes. *Organometallics* **2021**, *40* (17), 3033−3041.
(61) Ge, Y.; Lu, Z.; Dai, S. Flexible Axial Shielding Strategy for the Synthesis of High-Molecular-Weight Polyethylene and Polar Functionalized Polyethylene with Pyridine-Imine Ni(II) and Pd(II) Complexes. *Organometallics* **2022**, *41* (15), 2042−2049.
(62) Guan, Z.; Cotts, P. M.; McCord, E. F.; McLain, S. J. Chain Walking: A New Strategy to Control Polymer Topology. *Science* **1999**, *283* (5410), 2059−2062.
(63) Zhang, D.; Nadres, E. T.; Brookhart, M.; Daugulis, O. Synthesis of Highly Branched Polyethylene Using "Sandwich" (8-p-Tolyl naphthyl α-diimine)nickel(II) Catalysts. *Organometallics* **2013**, *32* (18), 5136−5143.
(64) Fall, W. S.; Baschnagel, J.; Lhost, O.; Meyer, H. Role of Short Chain Branching in Crystalline Model Polyethylenes. *Macromolecules* **2022**, *55* (19), 8438−8450.
(65) Galland, G. B.; de Souza, R. F.; Mauler, R. S.; Nunes, F. F. 13C NMR Determination of the Composition of Linear Low-Density Polyethylene Obtained with [η3-Methallyl-nickel-diimine]PF6 Complex. *Macromolecules* **1999**, *32* (5), 1620−1625.
(66) O'Connor, K. S.; Lamb, J. R.; Vaidya, T.; Keresztes, I.; Klimovica, K.; LaPointe, A. M.; Daugulis, O.; Coates, G. W. Understanding the Insertion Pathways and Chain Walking Mechanisms of α-Diimine Nickel Catalysts for α-Olefin Polymerization: A 13C NMR Spectroscopic Investigation. *Macromolecules* **2017**, *50* (18), 7010−7027.
(67) Pei, L.; Liu, F.; Liao, H.; Gao, J.; Zhong, L.; Gao, H.; Wu, Q. Synthesis of Polyethylenes with Controlled Branching with α-Diimine Nickel Catalysts and Revisiting Formation of Long-Chain Branching. *ACS Catal.* **2018**, *8* (2), 1104−1113.
(68) Jiang, S.; Zheng, Y.; Oleynik, I. V.; Yu, Z.; Solan, G. A.; Oleynik, I. I.; Liu, M.; Ma, Y.; Liang, T.; Sun, W.-H. N N-Bis(2,4-Dibenzhydryl-6-cycloalkylphenyl)butane-2,3-diimine-Nickel Complexes as Tunable and Effective Catalysts for High-Molecular-Weight PE Elastomers. *Molecules* **2023**, *28* (12), 4852.

https://doi.org/10.1021/acscatal.4c02708
ACS Catal. 2024, 14, 13136−13147